THEORETICAL MODELING OF BONDING CHARACTERISTICS AND PERFORMANCE OF WOOD COMPOSITES. PART IV. INTERNAL BOND STRENGTH

Chunping Dai*†

Senior Scientist and Group Leader

Changming Yu

Visiting Professor
FPInnovations – Forintek Division
2665 East Mall
Vancouver, BC
Canada V6T 1W5

Juwan Jin

Associate Professor
Nanjing Forestry University
Nanjing, Jiangsu
China

Abstract. A mechanistic model was developed to predict the internal bond (IB) strength of wood composites. Based on the earlier models reported in this series, the IB model integrates the mechanisms of inter-element contact, resin distribution, and localized bond development and debonding failure. Experimental tests were also conducted, and the results compare favorably with model predictions. It was discovered that a composite product having large horizontal density variations typically realizes less than 50% of the bond strength attainable between its constituent elements. The loss of bonding strength is attributed to the premature debonding of low-density regions, and the subsequent load concentration and failure-acceleration of the higher-density regions. The model predicts IB as a function of product density, wood density, resin content, and element dimensions. The IB improves with an increase of product density, resin content, and element thickness. The relationships are monotonic and nonlinear, resulting from their interactions on the contact development or/and the resin coverage. The relationship between IB and wood density is also nonlinear and dependent upon the product density. Implications of the predictive results on fundamental understanding and optimization of wood composite bonding are discussed.

Keywords: Modeling, simulation, wood composites, mechanical properties, bonding, internal bond strength, density, structure.

INTRODUCTION

The IB strength of a wood composite is defined as the ultimate failure stress of a wood composite panel under tensile perpendicular-to-plane loading. IB is a standard test (CSA 1993; ASTM 1989) that is commonly used for determining the bonding performance of non-veneer composite products such as particleboard, medium density fiberboard (MDF), and oriented strandboard (OSB).

Because it is an essential property of wood composites, IB has been broadly studied and reported (eg, Kelly 1977; Hsu 1995; Xu and Steiner 1995; Brochmann et al 2004). Almost all studies found in the literature are empirical. Theoretical or mathematical modeling of IB is basically nonexistent. More analytical approaches

---

* Corresponding author: dai@van.forintek.ca
† SWST member

are needed to fundamentally understand and further advance the science of wood composites.

In the previous papers of this publication series, we have modeled some of the essential aspects of wood composite bonding, including: contact between the constituent elements (Dai et al 2007), resin distribution over the element surfaces (Dai et al 2007a), and bonding strength between two elements/strands (He et al 2007). These works set a stage for the development of a comprehensive model to predict the IB strength of wood composites.

The specific objectives of this paper are:

To develop a mechanistic model to predict IB strength of wood composites,

To conduct experimental tests to determine the relationship between IB strength and panel density,

To validate the model by comparing the model predictions and the experimental results, and

To present the typical predicted results and discuss their implications on wood composite manufacturing.

MODEL DEVELOPMENT

A wood composite panel is modeled as a consolidated assembly of wood strands. The strands are randomly formed in a layered structure in which the major faces of the strands are parallel to the plane of the panel. Localized bonds are developed wherever interfacial contact and resin coverage are present. To link the global bonding strength to the behavior of local bonds, a spring-field model is used.

A spring-field model

Due to the complex internal panel structure and the orthogonal strength characteristics of wood, an out-of-plane tensile loading can induce a complex three-dimensional distribution of different stresses among wood strands: tension, shearing, and even compression. Figure 1 shows a one-dimensional IB model, which considers only tensile stresses. A wood composite panel (specimen) is viewed as a system of parallel-arranged springs. Each spring represents a column of bonded wood strands. The number of strand overlaps i in a given column and its relative column area $p(i)$ follow the Poisson distribution and have been analytically defined by the mat formation model (Dai and Steiner 1994; Dai et al 2005). Note that for some columns, overlap number i may be too low to form significant bonds (see broken springs in Fig 1). Under out-of-plane tensile loading σ, the springs extend to the same strain ε, but different stresses σ_i because of their different MOE, E_i. Note that i is both the index counter and the number of strand overlaps of a column. The variation of E_i is due to the variation of column-strand overlap. In fact, E_i should also vary with the vertical position of individual strands, if the vertical density profile is to be considered. Here we only consider a flat vertical density profile. Within a column, properties including elasticity E_i, stress σ_i, and bonding strength $[\sigma]_i$ are assumed to be uniform. The bonding strength between two strands was previously defined in terms of the relative contact area β_i, resin coverage R_a, and wood strength $[\sigma]_w$ (He et al 2007). Later we will demonstrate that such a treatment is practically sufficient for predicting IB strength of panels with a normal vertical density profile if the core density is used instead of the average panel density.

The IB strength is calculated using an iterative procedure through a numerical model written in Fortran. Figure 2 is a flowchart depicting the modeling logic. The local applied stresses σ_i and allowable stresses $[\sigma]_i$ need to be first obtained for given global loading. At each stress increment $\Delta\sigma_i$, localized debonding occurs if $\sigma_i > [\sigma]_i$. The debonding should begin in columns with lowest strand overlaps i_{min}. After a column fails, the load-sharing area is reduced, and the total load is then redistributed to the remaining columns. As the load continues to increase, the local stresses will increase, which may cause further debonding failures, and loss of supporting columns. At some point, the total load will
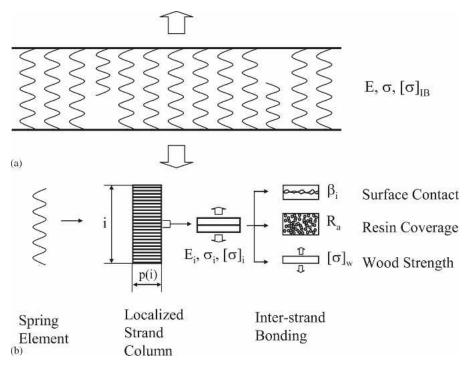
FIGURE 1. Schematic of the IB model. (a). A parallel spring-field model, and (b). Linkage between localized column of bonded strands, surface contact, resin coverage, and wood strength. Note that *i* is both the index counter and the overlap number of a column.

start to drop because of too many bond failures. The maximum loading stress will be deemed the IB strength, while the actual load may continue to decline until catastrophic failure, leading to the failure of the last column with the highest strand overlaps i_{max}.

Local stress distribution

According to the law of mechanical equilibrium, the global force F always equals the summation of forces in individual columns f_i, or:

$$F = \sum_{i=i_{min}}^{i_{max}} f_i \qquad (1)$$

where:

i_{min} = minimum column strand overlaps, given by the ratio of panel thickness T over initial strand thickness τ_0, or T/τ_0, and

i_{max} = maximum column strand overlaps, given

by the ratio of mat thickness T_0 over strand thickness τ, or T_0/τ_0.

Since the force is the product of stress and loading area, Eq (1) can be rewritten as:

$$\sigma = \sum_{i=i_{min}}^{i_{max}} p(i)\sigma_i \qquad (2)$$

where:

σ, σ_i = global and column stresses, respectively, and

$p(i) = a_i/A$, namely, probability density of the Poisson distribution of mat formation. Here a_i and A are the column and panel areas, respectively. The Poisson probability density is a function of panel compaction ratio and thickness ratio (Dai et al 2005). Equation (2) indicates that the global tension stress equals the weighted average of the column stresses, with $p(i)$ merely being the weighting coefficient.
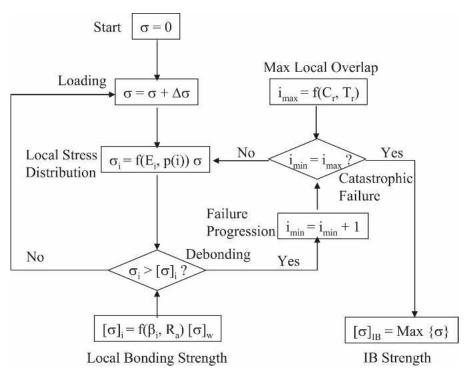
FIGURE 2. Flowchart of the computer model showing the logics of IB calculation.

On the other hand, the strain of the panel ε and the strain of individual columns ε_i are always the same between the panel and the columns, or:

$$\varepsilon = \varepsilon_i \qquad (3)$$

Therefore, Eq (2) can be further written as:

$$E = \sum_{i=i_{min}}^{i_{max}} p(i)E_i \qquad (4)$$

where E and E_i are elasticity of the panel and the columns, respectively.

One of the interesting findings that we obtained in this study was the *softening effect* of pressing on out-of-plane tensile MOE. The tensile elasticity of wood strands or bonded-wood strands E_i *decreases* with an increase of densification ρ_i, or:

$$E_i = \left(\frac{\rho_i}{\rho_0}\right)^m E_0 = \left(\frac{i\tau_0}{T}\right)^m E_0 \qquad (5)$$

where:

$E_0, \rho_0 =$ MOE and density of wood strands prior to pressing,

$i =$ number of column strand overlaps, and
$m =$ elasticity softening index ($m < 0$), also determined through fitting a regression between the data on E_O and E_i (see the experimental section).

Combining Eqs (2), (4), and (5), we can calculate the distribution of the column stresses σ_i at a given global stress σ using the following equation:

$$\sigma_i = \frac{i^m}{\sum_{i=i_{min}}^{i_{max}} i^m p(i)} \sigma \qquad (6)$$

Equation (6) shows that the local (column) stresses depend on not only the global stress but also the local elasticity, which in turn is affected by the column strand overlaps and softening index due to pressing. Contrary to general intuition, the more-dense columns are softer and hence realized lower pulling stresses than the

lower-density columns, due to the softening effect.

Strand-to-strand bonding strength

The local column stresses are supported by the strand interfacial bonding strength. The bonding strength between two overlapped strands is (He et al 2007):

$$[\sigma]_i = \beta_i R_{a2}[\sigma]_w \qquad (7)$$

where:

$[\sigma]_i, [\sigma]_w$ = bonding strength and transverse tensile strength of wood strands, respectively,

β_i = relative contact area between the strands, and

R_{2a} = total resin coverage between the strands. Note that the details on β and R_{a2} were given in Part 3 (He et al 2007).

To account for the effect of strand-edge voids on the loss of surface contact (Dai et al 2007), Eq (7) is modified as:

$$[\sigma]_i = \left(1 - \frac{a_{i,loss}}{a_{strand}} \right) \beta_i R_{a2}[\sigma]_w \qquad (8)$$

where $a_{i,loss}$ and a_{strand} are the area loss and strand surface-area, both detailed in Part I (Dai et al 2007).

Failure process and IB strength

Once the stress in a column σ_i (Eq (6)) reaches the corresponding bonding strength $[\sigma]_i$ (Eq (8)), a localized failure is assumed to occur in the form of debonding. The debonding should start with the weakest column that contains the fewest strand overlaps i_{min}. Note that i_{min} must be greater than T/τ to achieve adequate contact. A debonded column is then removed from the load support, and the load-bearing area is consequently reduced by the column area $\beta_i R_{a2} a_i$. The model employs the following failure criteria:

$$i_{min} = i_{min} + 1 \qquad (9)$$

if:

$$\sigma_i \geqq [\sigma]_i \qquad (10)$$

The loss in load-bearing area leads to the redistribution of load within the surviving columns. The localized stresses are expected to increase according to Eq (6), at one fewer supporting column. The increase of stresses may or may not result in further debonding. Nevertheless, as the load continues to increase, more columns will fail, leaving fewer columns to carry the load. Hence, the load-carrying capacity will drop. At a certain point in the loading-debonding process, the global stress σ will reach a maximum before it starts to drop leading to catastrophic failure. This maximum stress is deemed to be the IB strength $[\sigma]_{IB}$, or,

$$[\sigma]_{IB} = Max\{\sigma\} \qquad (11)$$

EXPERIMENTATION

Raw materials

Commercial aspen (P*opulus tremuloides*) strands from an OSB plant were used for board making. All the strands were dried in an oven to achieve a final moisture content of 2–3% based on oven-dry weight. Fines and small strands were removed by screening. A total of 100 screened strands were randomly sampled and measured for their average thickness, length, and width using a caliper and a ruler.

Water was added based on the moisture content of each batch of dry strands to maintain the final moisture content after blending at 6.5% based on oven-dry weight. Phenol-formaldehyde liquid resin and emulsified wax for commercial production were used. The application levels of resin and wax were 3.5 and 0.5% respectively based on the oven-dry weight of strands.

Measurement of out-of-plane tensile MOE of wood strands

Aspen strips were cut into 25- × 25-mm square strands. Two wood strands were overlapped without resin and hot-pressed using a mini press.

The pressing temperature was set at 200°C and pressing time was 60 s under various compaction ratios. The thickness of each pressed strand was measured. The strand was glued to aluminum blocks from both surfaces with a hot-melt adhesive. The tensile MOE of control strands E_O and that of pressed strands E_i were then tested using an Instron material testing machine. The loading speed for this test was set at 0.5 mm/min.

Panel fabrication

Uniformly-densified strandboards (U-SB). To produce uniformly densified strandboards (referred to as U-SB), a special pressing schedule was developed to keep the vertical density profile (VDP) as flat as possible. Similarly to the cold-prepressing method used for making uniform particleboard (Wong et al 1999), mats of resinated strands were pressed using a warm schedule prior to the full application of heat. Board density ranged 400–1000 kg/m³ in which a total of 8 nominal density levels were targeted with 3 replicates. Strands were randomly oriented via hand-forming into 610-mm × 610-mm mats. All mats were prepressed to the nominal target thickness of 11.1 mm at a platen temperature of 60 ± 1°C except for the highest density mats. For target panel density of 1000 kg/m³, the mats were pressed to the target thickness at 75°C to increase the compressibility of the mat. All mats were then held at the target thickness until the core reached the target prepress temperature. Then, both the top and bottom platens were heated to 170°C. The boards were removed as soon as the core reached 125°C. The whole pressing cycle lasted for 1200–1500 s for strandboards with different densities. The maximum mat pressure reached about 7 MPa. At such a high pressure, wood damage could occur and hence lower the IB. However, according to Carll and Wang (1983), the reduction of IB is insignificant.

Conventional strandboard (C-SB). As a control, strandboards with different average density ranging from 500–700 kg/m³ were also made by a conventional hot-pressing method. Strands used to fabricate C-SBs were obtained from the same blending batch used for the U-SBs. The size of the mat and the board replications at a given density level were similar to those for U-SBs. The hot-pressing temperature was 175°C and the pressing cycle was 400 s.

Evaluation of panel properties

The boards were trimmed to 533 × 533 mm and then were conditioned for 1 wk in a standard conditioning chamber (65% RH and 20°C) before being cut into test samples. For each board, 6 samples were prepared for the VDP determination and 12 for the IB test. The sample dimensions of 50 × 50 mm were based on the CSA O437.1–93 standard. Prior to testing, all the samples were further conditioned at 65% RH and 20°C. The VDP was tested using an X-ray scanner, while the IB was evaluated using an Instron testing machine.

RESULTS AND DISCUSSION

Model validation

Input parameters. Table 1 lists main input parameters for the model. The dimensions and densities for strand and panel are needed to define internal panel structure, including the random-strand overlap distribution i_{min}, i_{max}, $p(i)$, the local strand-to-strand contact β_i, and the relative bonded area, *RBA*. Mat moisture content

TABLE 1. *Main input parameters.*

Strand dimensions	
—	Length, λ: 101.6 mm
—	Width, ω: 25.4 mm
—	Thickness, τ_o: 0.762 mm
Wood (aspen strand) properties	
—	Density, ρ_w: 400 kg/m³
—	MOE before pressing, E_0: 5.0 MPa
—	Softening power index, m: −1.23
—	Transverse tensile strength, $[\sigma]_w$: 3.0 MPa
Board (mat) conditions	
—	Moisture content, MC: 5.0%
—	Resin content, R_c: 3.5%
—	Thickness, T: 11.1 mm
—	Density, ρ_b: 600 kg/m³

and resin content are input parameters for calculating resin coverage R_a and R_{a2}. The mechanical properties of strands are required to calculate the local stress σ_i, bonding strength $[\sigma]_i$, and the global bonding strength $[\sigma]_{IB}$.

In addition, typical vertical density profiles in the panels are needed. Figure 3 shows a flat density distribution across the panel thickness in the U-SB panels (Fig 3a), and higher-density surface layers and lower-density core in the C-SB panels (Fig 3b). The different density profiles should produce different IB-density relationships.

Model predictions vs experimental data. Figure 4 depicts the relationships between IB strength and board density. Three sources of results are compared: average IB strength of U-SBs, average IB strength of C-SBs, and predicted IB strength. In general, the IB of conventional strandboards increase in a linear manner with the average board density. However, the IB-density relationship becomes nonlinear if the core density is used instead of the average density. In
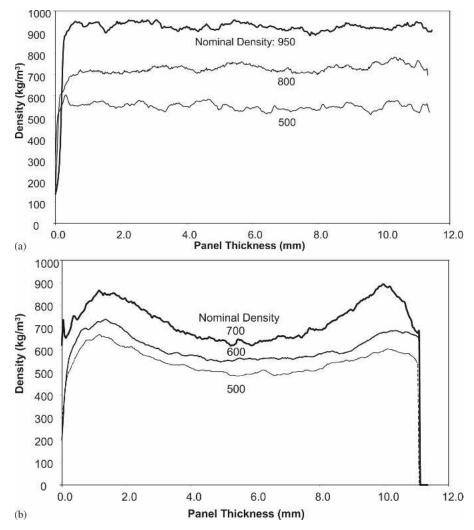

FIGURE 3. Vertical density profiles of laboratory-made strandboards. (a). Specially pressed uniform density profiles, and (b). Conventional vertical density profiles.
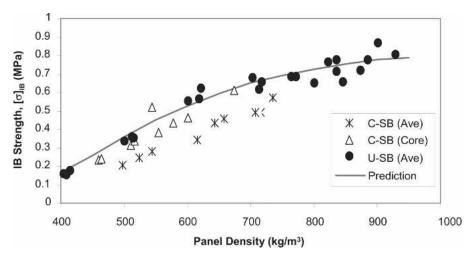
FIGURE 4. Comparing IB strengths between the model predictions and the experimental data.

fact, the IB-core density relationship closely overlaps with the IB-density data of U-SBs. Both agree well with the model predictions. This result implies that the model can be used to predict IB of both uniformly densified strandboards if the average board density is known, and conventional boards as long as the core density is used.

Bonding and debonding mechanisms

Difference between panel IB strength and strand-to-strand bonding strength. Figure 5

compares the predicted bonding strengths of an aspen-strand panel with those of two overlapped aspen strands, based on which predictions are made. At the same densification and resin content, the bonding strengths between two strands are, for the most part, more than double the IB strength of the panel. This result has several implications. First, the model can be used to simplify the complex and often expensive evaluations of adhesive and species interaction. Experimental tests of two wood strands bonded with a given adhesive system are much simpler
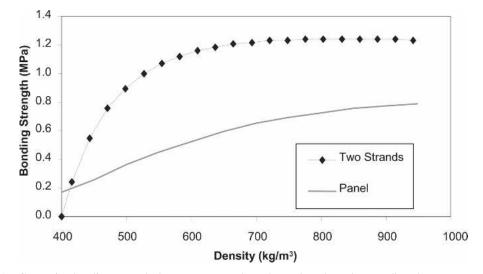

FIGURE 5. Comparing bonding strengths between two overlapped strands and regular strandboards.

than full-board tests. The results can be used as an input to the model to predict board-bonding properties, thereby minimizing board tests. Second, from the viewpoint of material structure, the bonding of two flat-strands more or less represents the class of veneer-based products, in which the constituent elements are continuous and uniform. On the other hand, the likes of OSB, MDF, and particleboard, due to their discontinuous and random structure, produce significantly lower bonding strength at a given densification than plywood and laminated veneer lumber.

More importantly, comparing the bonding strength between the composite product and its building blocks can shed light on the bonding mechanism. A strand panel typically has a large horizontal-density variation (Dai and Steiner 1997; Kruse et al 2000). In Part III (He et al 2007), we showed that the density and bonding strength relationship of overlapped strands is highly nonlinear. Within a panel, high-density areas are not proportionally high in bonding strength. In fact, the maximum local bond-strength is limited by the transverse tensile-strength of wood regardless of densification. Under out-of-plane tension, localized debonding failures can occur in the weakly-bonded low-

density areas even if the load is low. The premature debonding consequently leads to the load being concentrated in the higher-density areas, thereby weakening the overall load-carrying capacity. The debonding and load redistribution mechanisms are further analyzed in the following sections.

Localized tension MOE and bonding strength.
Figure 6 shows that the local-strand overlap number in a typical strandboard, 11.1 mm thickness and 600 kg/m^3, made of 0.76-mm-thick aspen strands, varies from 15–37. The higher the strand overlaps, the more intimate the contact between the strands, and thus the greater the localized bonding strength.

However, an opposite trend is observed with the tensile MOE. That is, the greater the overlaps, the lower the MOE. The softening effect, which is likely caused by buckling of the cell wall from densification, can have a significant implication on the local stress distribution and debonding process. Generally speaking, less-dense regions will have higher tensile elasticity and thus encounter greater stresses than the higher-density regions. This will lead to accelerated debonding failure in the weaker regions and reduced global IB strength of the panel. To further illustrate
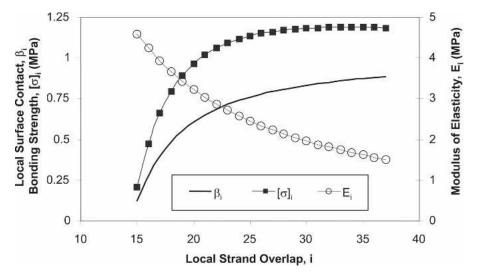

FIGURE 6.   Localized strand column properties as a function of strand overlap number.

this, Fig 7 depicts the predicted effect of different softening indices on IB strength. In particular, *m* equals 0 means no softening effect. That is, the MOE stays the same as the wood regardless of pressing. The *m* value of +1 means that there is a hardening effect from densification, and −1 represents a softening effect. The results confirm that the softening effect weakens the panel bonding strength.

Local stress distribution. Figure 8 depicts the variation of the allowable column stresses and actual stresses with column-strand overlaps. While the allowable stresses increase with strand overlaps, the actual stresses decrease with overlaps because of the previously-mentioned softening effect. At a global stress of 50 kPa, the column stresses are low and well below the allowable stresses. Therefore, there is no debonding failure. When the global stress increases to 200 kPa, the predicted stress in the 15-strand overlap-column exceeds the corresponding allowable stress. As a consequence, debonding failure occurs in that column. The load is redistributed, and the shared stresses in the remaining columns increase. Because only one column fails, the stress increases are very small. As the global stress increases, more columns will fail.

Figure 8 shows that the redistributed column stresses after the debonding failure at the global stress of 590 kPa are significantly greater than those at 450 kPa. The greater stress redistribution is also characteristic of the Poisson mat formation, ie, the relative area of the failed columns, becomes greater as the strand overlaps approach the average.

Variation of relative bonded area during debonding. The initial relative bonded areas (RBAs) depend primarily on the panel density and secondarily on other parameters such as wood density and strand thickness (Dai et al 2007). Figure 9 shows that during tensile loading, the RBAs decrease with the panel-loading stresses. The RBA-stress relationships clearly fall into two regions: progressive debonding and catastrophic failure. At the onset of loading, the stresses are relatively low and cause only weak bond sites (fewest strand columns) to delaminate. The debonding causes the RBAs to drop from the failed columns, the load to redistribute and concentrate in the surviving columns. With further increase of load, the next weakest columns will fail, and the subsequent process of load redistribution and concentration continues. During the progressive debonding process, the
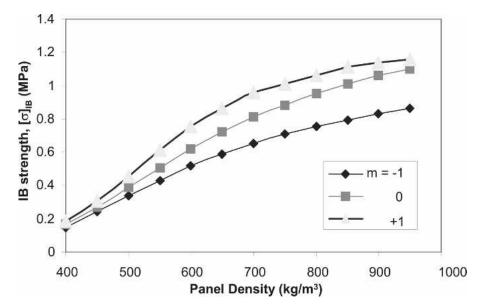

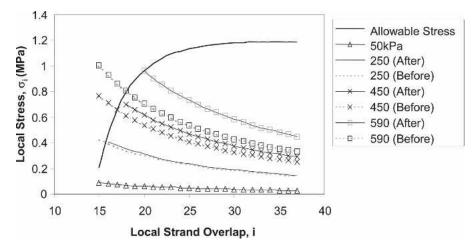FIGURE 7. Predicted effect of strand softening index on the IB strength.

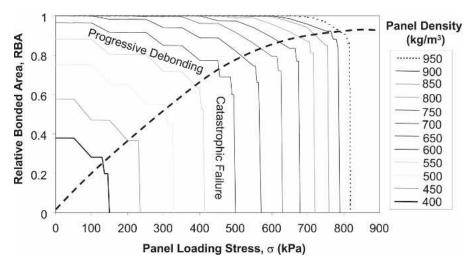FIGURE 8.   Predicted stress redistributions due to localized bond failures.

FIGURE 9.   Predicted changes of relative bonded areas during debonding and catastrophic failure processes (the values are in steps of 50 from 400–950 kg/m³ from left to right).

load continues to increase despite the steady decline of the RBAs, because the stresses of the remaining columns have yet to reach their corresponding bonding strengths. Once they do, catastrophic failure will occur in the form of sudden drop of RBAs. The global stresses immediately prior to failure are deemed to be the IB strengths. It is important to note that the maximum loads are supported by the RBAs which are significantly lowered from their initial values due to debonding. This is the direct cause to the degradation of IB strengths of composite

products compared with the bonding strengths of its constituents.

Typical predicted results

Effect of resin content on IB strength. It is generally known that IB increases with resin content (Kelly 1977). Figure 10 shows how the IB strength increases quantitatively with resin content at a wide range of panel density. A clear interaction exists between the resin content and the panel density. While IB increases with both
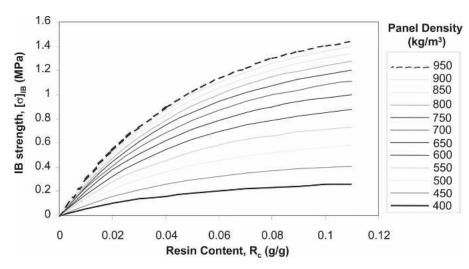
FIGURE 10.   Predicted effects of resin content on the IB strength at various panel densities.

variables, the rate of increase with resin content is largely controlled by panel density. The denser the panel, the more rapidly the IB increases with resin content. This is because a higher-density panel permits more intimate strand-to-strand contact, which, at a given resin coverage, means greater area for bonding (Eq (8)). The model predictions also confirm earlier findings concerning better resin efficiency at higher panel density reported in several experimental studies (Maloney 1970 and 1975; Kelly 1977). This result also implies that the bonding performance can gain more improvement from increasing resin usage in the more-dense surface layers than the lower-density core layers.

Effect of strand thickness on IB strength. Unlike resin content, the effect of strand thickness is generally not well defined in the literature. Some reported that thinner particles/strands were better for improving bonding strength (eg Meinecke and Klauditz 1962), while others found the opposite (Brochmann et al 2004; Hsu 1995). In theory, reducing strand thickness can lower void volume in the panel (Dai et al 2005), which helps promote surface contact for bonding (Dai et al 2007). On the other hand, thinner strands have greater surface area, which lowers the resin coverage (Dai et al 2007a). Then the question becomes: which effect is more domi-

nant. The model here takes into account both the effect of voids on contact and the effect of surface area on resin coverage and therefore is useful to quantify the net impact on the IB property.

As shown in Fig 11, the model predicts monotonic increases of IB with strand thickness. The result shows that increasing strand thickness always results in greater gain in resin coverage than loss of surface contact. The resin coverage factor seems to be more dominant when the strand thickness is <1 mm and when the panel becomes denser, as evidenced from the greater rate of IB increase. For typical oriented-strand products with density around 600 kg/m^3, the IB seems to gain the most with increasing strand thickness up to 1 mm. These results suggest that one may use thicker strand in the core to improve panel IB performance, while using thinner strands for the faces to improve surface quality and stress transfer for bending properties (Barnes 2001).

Effect of wood density on IB strength. Wood density is generally known as a variable having a direct effect on the bonding strength of wood composite panels. The adhesive bond is expected to be as strong as the wood substrate. Therefore more-dense wood normally gives higher bonding strength, as long as adhesive
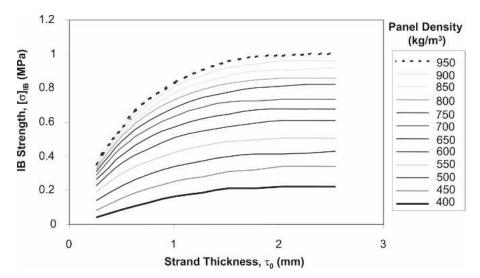
FIGURE 11. Predicted effects of strand thickness on the IB strength at various panel densities.

penetration and wood surface properties stay the same (Wellons 1981; Vick 1999; Widsten et al 2006). Part III of this series showed that the bonding strength between two bonded strands was proportional to perpendicular-to-grain tensile strength of wood (He et al 2007). Chow and Chunsi (1979) found that the shear bonding strength increased linearly with wood density before it reached 800 k/m^3. For these reasons, we assume the strand-to-strand bonding strength $[\sigma]_i$ increases proportionally with wood density

with a range of 300–600 kg/m^3, typically found in wood composites. Beyond this range, higher density may cause bonding problems due to reduced resin penetration and/or interference with high extractives often found in hardwood species (Chow and Chunsi 1979).

Wood density affects the IB strength of wood composite products in a complex manner as predicted in Fig 12. According to the model, a strong nonlinear interaction takes place between
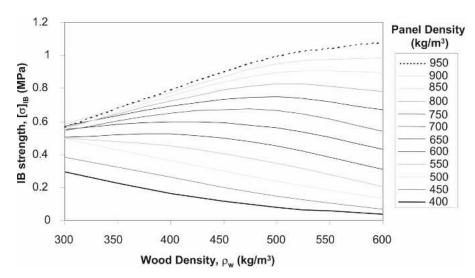

FIGURE 12. Predicted effects of wood density on the IB strength at various panel densities.

the wood density and the panel density. In particular, at lower panel density (below 600 kg/m^3), the IB deceases monotonically with wood density. This is because the loss of strand-to-strand contact dominates the gain of resin coverage with more-dense wood (Dai et al 2007 and 2007a). The model predictions agree with the experimental results obtained by Hse (1975), who studied the properties of particleboard made from hardwoods from southern pine sites. As the panel density increased beyond 600 kg/m^3, the IB starts to show trends of peaking at various wood densities before finally dropping. These results stem from the fact that greater resin coverage and wood strength (adhesive bond strength) can sometimes overcome the loss of surface contact if the panel density is sufficiently high. At very-high panel densities (ie, 900 kg/m^3 or higher), the IB increases monotonically with wood density, due to the existence of intimate contact. In view of vertical density profile, these results suggest that one may strategically place wood species according to the layer positions to achieve optimum performance of bonding and other properties of the pressed products.

SUMMARY AND CONCLUSIONS

Built upon the models of interelement contact (Dai et al 2007), resin distribution (Dai et al 2007a), and element-to-element bonding strength (He et al 2007), a comprehensive model was developed to predict IB strength of wood composites. The global IB strength was linked to local tensile stresses and bonding strength using a spring-field model. The model predicts IB strength as a function of resin content, element dimensions, wood density, and panel density. It captures the mechanisms of bonding and debonding in a random structure of wood composites. Experimental tests were conducted and the results agreed well with model predictions.

It was revealed that a composite product having large horizontal density variations realized less than 50% of the bond strength attainable between its constituent elements. The loss of bonding strength is largely attributed to the premature

debonding of low-density regions, and the subsequent load concentration and failure acceleration of the higher-density regions. The highest local bonding strengths are limited by the transverse tensile strength of wood constituents. Strong interactions exist between all the main variables affecting the IB: product density, wood density, resin content, and element thickness. The IB improves with increase of product density, resin content, and element thickness. The relationships are monotonic and nonlinear, resulting from their interactive effects on the contact development or/and the resin coverage. The relationships between IB and wood density are also highly nonlinear and dependent upon the product density. At lower product densities, IB decreases with increase of wood density due to insufficient contact. At higher product densities, IB increases first with wood density due to increased resin coverage and wood strength, and then decreases with further increase of wood density due to lack of contact.

The models presented in this series permit the complex bonding mechanisms of wood composites to be analyzed on a more fundamental ground. The concepts and proposed methodologies have opened a door for further modeling of wood composite bonding and other properties. These models help form a theoretical basis for design and optimization of wood composite products through manipulating such variables as: resin content, element dimensions, wood density, and product density.

REFERENCES

ASTM (1989) D 1037-Standard: Methods of evaluating the properties of wood-based fiber and particle panel material. Pp 167–196.

BARNES D (2001) A Model of the effect of strand length and strand thickness on the strength properties of oriented strand composites. Forest Prod J 51(2):36–46.

BROCHMANN J, EDWARDSON C, SHMULSKY R (2004) Influence of resin type and flake thickness on properties of OSB. Forest Prod J 54(3):51–55.

CSA (1993) O437.1-93: Test methods for OSB and waferboard. Pp 35–58.

CARLL CG, WANG P (1983) Data for prediction of mechanical properties of aspen flakeboards. USDA Research Note FPL-0246. Forest Products Lab, Madison, WI.

CHOW S, CHUNSI KS (1979) Adhesion strength and wood failure relationship in wood-glue bonds. Mokuzai Gakkaishi 25(2):125–131.

DAI C, STEINER PR (1994) Spatial structure of wood composites in relation to processing and performance characteristics. Part III. Modelling and simulation of a random multi-layered flake mat. Wood Sci Technol 28(3):229–239.

———, ——— (1997) On horizontal density variations in randomly-formed short-fibre wood composite boards. Compos Part A-Appl S 28(A):57–64.

———, YU C, ZHOU X (2005) Heat and mass transfer in wood composite panels during hot pressing. Part 2. Modeling void formation and mat permeability. Wood Fiber Sci 37(2):242–257.

———, ———, ZHOU C (2007) Theoretical modeling of bonding characteristics and performance of wood composites. Part I. Inter-element contact. Wood Fiber Sci 39(1):48–55.

———, ———, GROVES K, LOHRASEBI H (2007a) Theoretical modeling of bonding characteristics and performance of wood composites. Part II. Resin distribution. Wood Fiber Sci 39(1):56–70.

HE G, YU C, DAI C (2007) Theoretical modeling of bonding characteristics and performance of wood composites. Part III. Bonding strength between two wood elements. Wood Fiber Sci 39(4):566–577.

HSE CY (1975) Properties of flakeboards from hardwoods growing on southern pine sites. Forest Prod J 25(3):48–53.

HSU E (1995) Optimization of pressing parameters. Forintek Canada Corp. Technical Report, No 3812M215. 12 pp.

KELLY M (1977) Critical review of relationships between processing parameters and physical properties of particleboard. USDA General Technical Report FPL-10. Forest Products Lab, Madison, WI.

KRUSE K, DAI C, PIELASCH A (2000) An analysis of strand and horizontal density distributions in oriented strand board (OSB). Holz Roh-Werkst 58:270–277.

MALONEY TM (1970) Resin distribution in layered particleboard. Forest Prod J 20(1):43–52.

——— (1975) Use of short-retention-time blenders with large-flake furnishes. Forest Prod J 25(5):21–29.

MEINECKE E, KLAUDITZ W (1962) Physics and technology of bonding in particle-board production. Research report of North Rhine Westfalia No. 1053. Westdeautscher Verlag, Cologne and Opladen (Translated from German by Israel Program for Scientific Translations in 1968). 81 pp.

VICK CB (1999) Adhesive bonding of wood materials. *In*: Wood Handbook—Wood as an Engineering Material. USDA Forest Products Laboratory. Chapter 9. 24 pp.

WELLONS JD (1981) The adherends and their preparations for bonding. *In*: Adhesive Bonding of Wood and Other Structural Materials. USDA Forest Products Laboratory. 87–134.

WIDSTEN P, GUTOWSKI VS, LI S, CERRA T, MOLENAAR S, SPICER M (2006) Factors influencing timber gluability with one-part polyurethanes—studied with nine Australian species. Holzforschung 60:423–428.

WONG ED, ZHANG M, WANG Q, KAWAI S (1999) Formation of the density profile and its effects on the properties of particleboard. Wood Sci Technol 33:327–340.

XU W, STEINER PR (1995) Rationalizing internal bond and thickness swell test specimen size. Wood Fiber Sci 27(4):389–394.